

Foaming of AA 6061 using multiple pieces of foamable precursor

Isabel Duarte^{a,b,1}, Mónica Oliveira^a, Francisco Garcia-Moreno^{c,d}, Manas Mukherjee^{c,e},
John Banhart^{c,d}

^a *Department of Mechanical Engineering, University of Aveiro, Campus Universitário de Santiago, 3810-193 Aveiro, Portugal*

^b *TEMA - Centre for Mechanical Technology and Automation, University of Aveiro, Campus Universitário de Santiago, 3810-193 Aveiro, Portugal*

^c *Institute of Applied Materials, Helmholtz Centre Berlin, Hahn-Meitner-Platz 1, 14109 Berlin, Germany*

^d *Department of Materials Science and Technology, Technical University Berlin, Hardenbergstrasse 36, 10623 Berlin, Germany*

^e *Department of Metallurgical and Materials Engineering, Indian Institute of Technology Madras, Chennai 600 036, India*

1

Corresponding author. Tel.: +351 234 370830; Fax: +351 234 370953.

E-mail address: isabel.duarte@ua.pt (Dr.-Ing. I. Duarte).

Abstract

Aluminium foams were produced by expanding multiple pieces of foamable precursor inside a mould instead of using a single piece. The kinetics of foam formation and mould filling were visualised *in-situ* by X-ray radioscopy. It was found that foaming of multiple precursor materials leads to the best result when the growth directions of the individual precursor pieces are perpendicular to each other. X-ray tomography was used to study the internal structure of the foams in 3D. High local densities in joining regions and in areas of delayed pore nucleation were observed.

Keywords: Aluminium alloy foams; Multiple precursors; Powder metallurgy; X-ray radioscopy; X-ray tomography

1. Introduction

Complex near-net shape components of metal foam can be obtained by expanding inside a closed mould a single piece of foamable precursor material that is cut, e.g. from large extruded bars [1-4]. This can result in a considerable amount of clipped material and imply cost-driving material losses. Moreover, the production of large components requires the preparation of precursors of large dimensions which is more difficult than to make smaller ones using the conventional compaction techniques (e.g. isostatic hot compaction or extrusion). The production step of the precursor material has to ensure a homogeneous distribution of the blowing agent in the metallic matrix [5].

An alternative way is the production of components by using multiple precursor pieces instead of a single piece of precursor [6-12]. The Institute of Materials and Machine Mechanics [6] in cooperation with the company Mepura [7] were the first to exploit the possibility to use various pieces of simply shaped precursors (e.g., wires, granulate, etc.) for producing parts of different shapes (flat-, rod- or 3D-shaped). The company Alulight (Ranshofen, Austria) commercialised Al foam panels made by foaming many individual pieces of foamable precursor wire arranged in parallel or perpendicular in the mould, which gave rise to a typical surface pattern of grey shades [8]. Foaming using multiple precursors is influenced by a number of factors including the position of the precursor pieces, mould characteristics (material, geometry and dimensions), the temperature course, atmosphere and the details of solidification [4-5, 10]

The influence of both the shape and size of precursor granules on metal foaming behaviour was studied by Baumeister and Stöbener [9]. Foam expansion was

characterised in free foaming experiments, in an expandometer or by foaming in conventional moulds. They found that the shape, the surface/volume ratio and the surface quality of precursors have a significant influence on foaming. For example, the maximum expansion values were clearly lower for halfmoon-shaped particles than for disc-shaped particles, which was explained by both hydrogen losses via diffusion and the higher resistance against expansion of the surface oxides in the half-moon shaped particles. In general, higher surface/volume ratios (occurring for smaller precursor particle size) lead to higher densities of the foam due to a higher oxide content.

Solórzano et al. also worked on improving the foaming process of an aluminium alloy [10]. Production of metal foams through multiple precursors was addressed and observed that the appearance of foams made from a single piece of precursor and from multiple precursors varied with respect to surface roughness, degree of joining between various parts of a foam and the occurrence of collapsed zones.

Nosko et al. studied the effect of the initial location of the precursor material in the mould on structure and compression behaviour of the resulting foams *ex-situ*, i.e. by analysing solid foams after foaming [11]. The initial position of the precursors in the mould had a significant effect on the structure of the foam. These differences were attributed to changes of heat conduction and pore formation kinetics during foaming.

None of these studies showed what happens during foaming of multiple precursors and how 3D structures develop. Stanzick et al. monitored the joining of randomly placed precursor pieces in a mould during foaming by X-ray radioscopy [12].

They realised that during the merger of various foaming pieces inhomogeneous structures were obtained.

Our current work exploited more systematically X-ray radioscopy and tomography to observe and characterize metal foam structures during and after foaming. One task was to identify suitable arrangements of the precursor while taking into account their predominant growth direction. Mould filling and joining of foams were studied as well as the effect of possible expansion and temperature gradients due to different thermal contacts and the interaction between individual pieces of precursors.

2. Experimental

2.1. Materials

The foamable precursor material used in this study was obtained by mixing pre-alloyed AA 6061 powder with 0.5 wt.% titanium hydride powder (see also Ref. 5). The powder mix was first consolidated to cylindrical billets of 70 to 80% theoretical density by cold isostatic pressing. These billets were then pre-heated to temperatures between 350 °C to 400 °C and extruded to rectangular bars of 160×20 mm² cross-section in a second step in which the horizontal 25 MN direct extrusion machine at Honsel AG was used [13]. The resulting precursor material exhibited the typical anisotropies of a directional compaction process [5]. **Table 1** summarises the main properties of the powders.

Rectangular (8.5×8.5×5 mm³ in size) and wedge-shaped (base 10 mm, height 10 mm, depth 5 mm) samples of precursor material were cut off this panel in two directions

(parallel and perpendicular to the extrusion direction) to study two distinct foam growth directions in the mould. These samples were foamed inside a mould and observed by means of *in-situ* X-ray radioscopy. The effects of the initial position and orientation of the precursor pieces in the mould, their foaming direction and the influence of gravity on mould filling were observed. The foaming kinetics of each individual precursor piece was evaluated. More specifically, one or more pieces of precursor material were placed into a rectangular stainless steel mould with a cross section $16.6 \times 16.4 \text{ mm}^2$, wall thickness 1.5 mm and length of 11.6 mm. The two open ends of this mould were aligned in the direction of the X-rays and were delimited by two boron nitride (BN) plates (1.7 mm thickness) with low X-ray absorption. Different arrangements of multiple precursors with respect to the foam growth direction (parallel and perpendicular to the base of the mould) were tested to evaluate in which way a single aluminium alloy foam can best be made.

2.2. X-ray radioscopy

A laboratory X-ray radioscopy set-up comprising a microfocus X-ray source and a flat panel detector was used to record the foaming process *in-situ* [14-16]. The X-ray spot size was set to $5 \text{ }\mu\text{m}$ while applying 100 kV voltage and $100 \text{ }\mu\text{A}$ current. The pixel size of the flat panel detector – area $120 \times 120 \text{ mm}^2$ – was $50 \text{ }\mu\text{m}$. As the magnification used was set to 4-fold, the pixel size in the radiographic images corresponds to $12.5 \text{ }\mu\text{m}$. 2D X-ray projections of $2240 \times 2368 \text{ pixel}^2$ each were recorded of the foam every 2 s using the commercial software HiPic version 7.1 by Hamamatsu. Images were analysed using the software package AXIM that is based on the commercial program PV-WAVE and allows one to analyse the expansion of a foam quantitatively [14, 16]. AXIM separates darker object pixels from brighter pixels above and below the object and from black pixels of

the sample support. Object pixels can be separated from the environment by applying threshold criteria [16]. The images were converted into binary images (black and white) after which the geometrical variations of the sample during foaming were determined. The projected area of a foam (A) at a given time normalised by that of the initial precursor (A_0) is defined as “area expansion” (A/A_0). Area expansion is smaller than volume expansion if we allow the foam to expand in the X-ray direction, but by consistently using area expansion, a quantitative comparison between various samples can be made without knowing the value of volume expansion.

Foaming was performed in a furnace heated by light from two halogen photoptic lamps of 150 W heating power (Osram Xenophot HLX 64635) focussed by an IR reflector. The closed rectangular mould containing the precursor was placed in the middle of this lamp furnace on a ceramic plate which kept heat losses by conduction low. The centre of the steel mould’s bottom surface had a hole through which a K-type thermocouple was inserted for measuring the temperature of the expanding foam. The precursor samples were heated up to 640°C and were held there for a few minutes. For every sample, foaming was stopped after the X-ray image indicated that the foam had completely filled the mould. Images were also acquired during cooling.

2.3. X-ray computer tomography

Computed X-ray tomography is suitable for investigating the 3D structure of foams [17-21]. We performed X-ray tomography for analysing the foam structure using the same X-ray source as for radioscopy. A foam was placed on a motor-controlled rotating table in between the X-ray source and detector. The foam was rotated around its

vertical axis through 360° in 1300 steps while acquiring radiographic images after each step. Three-dimensional (3D) reconstruction of the data was performed using the software Octopus [22]. The software VGStudioMax 1.2.1 was used to extract 2D and 3D sections of the foam from reconstructed data.

3. Results and discussion

3.1. Foaming behaviour of single pieces of precursor material

Fig. 1 shows representative temperature and expansion profiles of the precursor material with foam growth perpendicular to the mould base. This expansion curve is typical for these aluminium alloys and can be divided into four regions [5]: I) a small initial expansion for temperatures below the solidus temperature, followed by II) an increase of expansion as a consequence of the decomposition of TiH_2 to hydrogen gas and the softening of alloy taking place in parallel, III) rapid increase of the expansion rate as the temperature increases until a maximum expansion is reached ($[A/A_0]_{\max} = 3.18$), and IV) onset of foam collapse as the blowing agent is exhausted and no longer releases sufficient hydrogen to counterbalance losses.

The effect of the foam growth direction on foaming behaviour and on mould filling was studied using rectangular samples ($8.5 \times 8.8 \times 5 \text{ mm}^3$) that were prepared to foam in two distinct ways – perpendicular or parallel to the mould base – as exemplified in **Fig. 2**. The radiosopic images for all cases reveal that the shape of the bubbles varies during foaming in a similar way.

Three stages occur, namely bubble nucleation, bubble growth and foam collapse [5]. Voids initially appear as cracks aligned perpendicular to the foaming direction (parallel to the mould base in **Figs. 2a** and **2c**, perpendicular in **Fig. 2b** and then first change to spherical and then to polyhedral shape [5]. More spherical bubbles are observed when the expansion reaches the maximum value (see, e.g., $t = 380$ s in **Fig. 2a**).

The foam structure is similar in all three cases. Gravity does not have a notable effect on structure formation until maximum expansion has been reached. The main differences between the three experiments are associated to foam stability, collapse mechanism (coalescence or drainage) and metal redistribution. The foam made from a precursor with a foam growth direction parallel to the mould base (**Fig. 2b**) shows a more pronounced collapse induced by a stronger coalescence rate and a slight drainage effect (**Fig. 2b**). Drainage and coalescence lead to the formation of a denser metal layer at the bottom of the foam and large bubbles on the top, respectively (**Fig. 2b**). The final projected shape of the foams depends on the direction of foam growth. It is near-circular (**Fig. 2a**) or elliptical (**Fig. 2b**) for foam growth perpendicular or parallel to the mould base, respectively. The precursor expands up to the top of the mould in **Fig. 2c**, whereas the precursor in **Fig. 2b** expands towards both lateral sides of the mould symmetrically without constraints until it touches the mould walls. Therefore, this type of precursor is most suitable for filling a long horizontally arranged hollow section in which the precursor is placed in the middle of the profile. However, the structure of such foams is not satisfactory due to effects of drainage as well as of foam flow impaired by friction with the walls of the section [23-24]. It has been claimed that radial expansion is most suitable for filling hollow profiles [24]. **Fig. 2c**, where the precursor is tilted by 90° ,

shows that even when gravity is oriented along the expansion direction, there is no change in drainage profile. The tilting in the course of expansion is due to its high height to width ratio. Bubble coalescence and drainage are more visible when foam growth is parallel to the base of the mould, see **Fig. 2b**.

The effect of foam growth direction on the density profile during foaming is presented in **Fig. 3**. The density profile in **Fig. 3a** indicates no drainage, while slight drainage (dashed red oval) is observed in **Fig. 3b**. The different foam growth directions – parallel and perpendicular to the mould base – are associated with different modes of heat transfer. The sample with a foam growth direction parallel to the mould base receives increasingly more heat during foaming due to a growing contact area and therefore drainage can be higher. Moreover, the balance between gravity, capillary forces, disjoining pressure and hydrogen pressure inside the bubble is also different [5].

Fig. 4 shows representative X-ray radioscopic images of differently positioned wedge-shaped precursor pieces. The foam growth direction is parallel to the base of the mould. The final foam exhibits rounded contours for both samples. Such shapes are formed irrespective of the initial shape of the precursor (rectangular or triangular) for free foam expansion. The sample in **Fig. 4a** starts to foam earlier than the sample in the **Fig. 4b** due to faster and more stable heating conditions.

3.2. Foaming using multiple pieces of precursor material

Different ways of precursor arrangement are studied. The studies are grouped into two main arrangements based on the growth direction of the precursors with respect to

the mould: (i) all pieces of precursor material have the same foam growth direction (**Fig. 5**). (ii) individual precursor materials have different foam growth directions (**Fig. 6**).

Fig. 5 demonstrates the foaming of various pieces of precursor material that have the same foaming direction. In **Figs. 5a and 5b** the precursors expand in a direction perpendicular to the base of the mould, i.e. parallel to gravity: two pieces positioned side by side in the mould (**Fig. 5a**), or three pieces, where two of the pieces are placed side by side and the third on top of the first two samples (**Fig. 5b**). **Fig. 5c** presents the foaming behaviour of two precursor pieces placed one above the other, where the foam growth direction is parallel to the base of the mould and perpendicular to gravity. No complete mould filling is obtained using precursors growing in the same direction, see the images of the final foam on the right. Joining of the foams may be very strong locally as foams appear darker, i.e. denser, see the acquired radioscopic images at 500 s in **Fig. 5b**. In the first two cases (**Figs. 5a and 5b**), joining between the individual foams is different to **Fig. 5c**, see photograph on right side. Each individual precursor piece starts to foam individually until the pieces touch each other on one (**Fig. 5a**) or more sides (**Fig. 5b**). The latter situation promotes joining between different foams since the relative movement of two foams with respect of each other helps to shear off oxide layers and promotes metallic bonding. In contrast, slowly moving faying foam surfaces tend to remain separated by oxide films after solidification. It is also observed that the precursors do not start to foam at the same time. This is due to temperature gradients inside the closed mould where the walls of the moulds are regions of higher temperature and different thermal contacts of the precursor pieces. This is visible for precursor pieces stacked on top of each other in the middle of the mould, as shown in the images for 186 s

and 298 s in **Fig. 5b** and **Fig. 5c**, respectively. Moreover, foaming of a piece of precursor can influence the foaming of its neighbours as seen in **Fig. 5c**. Pore nucleation starts in the bottommost precursor and spreads to the top precursor towards the top mould wall (see images for 212 s and 500 s in **Fig. 5c**). The arrangement in **Fig. 5c** gives rise to more drainage with a formation of a dense metal layer at the bottom of the lower formed foam, see arrows in **Fig. 5c**. This is due to the weight of the upper precursor as well as the foam growth direction perpendicular to gravity. The weight of upper precursor modifies the typical shape of the bottom foam. There is no joining between the foams in this case.

Fig. 6 shows the foaming of three pieces of precursor material. Here, the pieces in the mould have different foaming directions. From the radioscopic images it is observed that the rectangular mould is completely filled by the foam for all the different arrangements of precursors, see the images corresponding to the times of 238 s, 258 s and 238 s, in **Fig. 6a**, **Fig. 6b** and **Fig. 6c**, respectively. The mould is filled in a non-uniform way. Initial foaming depends on the position of the precursors. The pieces closer to the mould walls (lateral and top sides) start to foam earlier than the ones at the bottom of the mould, thus implying a thermal gradient caused by the reduced thermal contact between samples, that gives rise to a non-uniform cell size distribution and density variations. The oxide layers covering the precursors and the air gaps between them act as thermal bridges and also contribute to non-uniform pore nucleation by further reduction of heat transfer between the precursors. The result is the formation of a non-uniform foam structure with areas of markedly different pore sizes and shapes and different density, see the images corresponding to the times of 238 s, 258 s and 238 s, in **Fig. 6a**, **Fig. 6b** and **Fig. 6c**, respectively. The top of the mould is filled first and towards the end of foaming,

overheating of the upper part again produces a region of lower density. This is the reason for the asymmetric density profile. Nevertheless, the arrangements using precursor pieces with different foaming directions are the most satisfactory configuration for mould filling.

The results demonstrate that each precursor piece expands individually within the mould in a direction perpendicular to the extrusion direction. For a given time, the different foaming pieces can be in different foaming stages (nucleation, pore growth and collapse). For example, for $t = 198$ s (**Fig. 6c**), there are two foams (A, B) in the nucleation stage (porosity resembles cracks aligned perpendicular to the foaming direction) and one foam (C) in the pore growth stage (shape of the bubbles is spherical). Foam B is more delayed than Foam A. The radioscopic images also reveal that joining between the different foams should be achieved before the collapse stage starts because otherwise the foams develop zones showing more pronounced coalescence effects. For example, joining between foam I and foam II in **Fig. 6a** (see acquired image at 198 s) is still achieved with spherical bubbles in which the junction region is not visible (see region III in the acquired image to 238 s). The junction region is not observed in region IV, see the acquired image to 244 s, in **Fig. 6b**. In both examples, regions III and IV show a homogeneous distribution of spherical cellular pores and a uniform metal distribution because both pieces foamed similarly and their interfaces touched in an early foaming stage. Although the pores in the initial stages are small and spherical, they become large and irregular after extended heating.

Better joining between two precursors is achieved by placing such that their foaming directions are perpendicular to each other. In this way, we force both formed

foams to join in initial stages of foaming. This effect can be observed in **Figs. 6a** and **6b** for the times 238 s and 244 s, respectively. Here, the merged regions between the two foams formed are not visible by contrast variations. In all the samples, a non-uniform metal redistribution is observed by which a large amount of metal is located in the junction regions. Joining between various foams is impaired by the outer oxide skin [5, 25-26].

The foaming process can be changed by the presence of neighbouring precursors as well as by gravity. For example, in **Fig. 6c**, foam A pushes foam B (see 198 s in **Fig. 6c**). The radioscopic images show that the precursor moves down during foaming as it softens and responds to gravity (see the acquired images to 198 s and 218 s in **Fig. 6a**).

These results demonstrate that multiple precursors should be placed into a mould in a defined arrangement to promote uniform foaming. Their growth directions should intersect with each other, thus forcing their interfaces to come into contact and to move relatively to one another. This can be observed by comparing the examples shown in **Fig. 5b** and **Fig. 6a** based on the same initial amount of precursor (three individual pieces). This observation demonstrates that symmetric heating of precursors (precursors start to foam at the same time) is required if one wants to obtain foam with a uniform structure.

The final foaming stage observed yields largely non-uniform rectangular foams with high-density regions located in the junctions (see the darker regions in the last radioscopic images that correspond to 518 s, 522 s and 410 s in **Fig. 6a**, **Fig 6b** and **Fig. 6c**, respectively). These density-increased regions could be explained by surface oxides or other contaminations. In an extreme case, this could lead to the formation of big voids

but usually, a slight density increase around the defects seems to be the only consequence (see the acquired image to 522 s in **Fig. 6b**). The low-density region results from the temperature increase at the end of mould filling due to the contact of the foam with an overheated upper mould wall. The life time of pores becomes shorter when the dwell time at a high temperature is too high.

Rectangular foams are produced using different arrangements of precursors with different foaming directions as shown in **Fig. 7** (see the black arrow). The samples have a similar appearance from the outside, characterised by a smooth surface. The joining region between the formed foams from the different precursors is usually visible [10].

3.3. X-tomography

Fig. 8 shows 2D cross sections of a solidified foam obtained using several multiple precursors. Different features can be detected: a region of small pores created from the precursor that is the last to expand and a region of large pores due to excessive time at high temperatures leading to foam collapse (see **Figs. 8a, 8b** and **8c**). The joining regions have a higher density (see small arrows in **Fig. 8**). Large voids could have formed if the joining between the foams is not fully achieved (see **Figs. 8b** and **8c**).

The result is the formation of a non-uniform foam structure with areas of significantly different pore sizes and shapes and different density (see **Fig. 9**). The 3D-images of the solidified foams in **Fig. 9** allow for a more detailed visualisation of these foams, especially the joining regions as well as the larger voids. These foams have cellular structures with pores of different sizes and geometries, structural defects and density gradients (see **Fig. 9**). Cells are mostly polyhedral or spherical. The cells in the

high-density region of the foam (junction region) are more spherical and small (**Fig. 8a** and **Fig.9a**).

4. Conclusions

X-ray radiography and tomography were used to visualise mould filling by metal foam and to investigate problems of technological relevance. Rectangular aluminium foam parts could be obtained by using multiple pieces of precursor. For better joining, multiple precursor pieces should be placed in such way so that the foam growth directions are perpendicular to each other. The effect of gravity on drainage is more pronounced when foaming is perpendicular to the gravity direction. Thermal gradients in the precursors are found to influence mould filling and to give rise to non-uniform cell sizes. Improved density distributions and more regular cellular structures can be produced when all precursor pieces start to foam simultaneously.

Acknowledgements

The authors wish to thank M.J. Amaral (Vale de Cambra, Portugal) for the preparation the precursor material samples for X-ray radiography tests. Support of ESA (MAP AO 99-075) is also acknowledged.

References

- [1] C.-J. Yu, H. H. Eifert, J. Banhart, J. Baumeister, Metal foaming by a powder metallurgy method: Production, properties and applications, *Mat Res Innovat* 2 (1998) 181–188.
- [2] H.P. Degischer, B. Kriszt, *Handbook of Cellular Metals*, Wiley-VCH, Weinheim, 2001.
- [3] J. Banhart, J. Baumeister, Production methods for metallic foams, in: D.S. Schwartz, D.S. Shih, A.G. Evans, H.N.G. Wadley (Eds.), *Materials-Research-Society Symposium on Porous and Cellular Materials for Structural Applications*, 13-15 April 1998, San Francisco, USA, *Mat. Res. Soc. Symp. Proc.*, 521, Materials Research Society, Warrendale, 1998, pp. 121–132.
- [4] I. Duarte, M. Oliveira, Aluminium alloy foams: production and properties, in: K. Kondoh (Ed.), *Powder Metallurgy*, Published by InTech, Rijeka, Croatia, 2012, pp. 47–72.
- [5] I. Duarte, J. Banhart, A study of aluminium foam formation - kinetics and microstructure, *Acta Mater.* 48 (2000) 2349–2362.
- [6] F. Simančik, J. Jerz, J. Kováčik, P. Minár, Aluminium foam - a new light weight structural material, *Kovove mater.* 35 (1997) 265–277.
- [7] H.P. Degischer, H. Wörz, German Patent DE 4206303 (1992).
- [8] Product data sheet of *Alulight*®, Alulight GmbH Ranshofen, www.alulight.com

- [9] J. Baumeister, K. Stöbener, Investigations on expansion behaviour of granulated foamable precursor material, in: J. Banhart, N. A. Fleck, A. Mortensen (Eds.) Cellular Metals: Manufacture, Properties, Applications, 23–25 June 2003, Berlin, Germany, Metall Innovation Technologie MIT-Verlag, Berlin, 2003, pp. 143–146.
- [10] E. Solórzano, J. A. Reglero, M.A. Rodríguez-Pérez, J. A. Saja, M.L. Rodríguez-Méndez, Improvement of the foaming process for 4045 and 6061 aluminium foams by using the Taguchi methodology, *J. Mater. Sci.* 42 (2007) 7227–7238.
- [11] M. Nosko, F. Simančík, R. Florek, Reproducibility of aluminum foam properties: Effect of precursor distribution on the structural anisotropy and the collapse stress and its dispersion, *Mater. Sci. Eng. A* 527 (2010) 5900–5908.
- [12] H. Stanzick, M. Wichmann, J. Weise, L. Helfen, T. Baumbach, J. Banhart, Process control in aluminium foam production using real-time X-ray radioscopy, *Adv. Eng. Mater.* 4 (2002) 814–823.
- [13] F. Baumgärtner, I. Duarte, J. Banhart, Industrialization of powder compact foaming process, *Adv. Eng. Mater.* 2 (2000) 168–174.
- [14] F. Garcia-Moreno, M. Fromme, J. Banhart, Real-time X-ray radioscopy on metallic foams using a compact micro-focus source, *Adv. Eng. Mater.* 6 (2004) 416–420.
- [15] F. Garcia-Moreno, M. Mukherjee, C. Jiménez, A. Rack, J. Banhart, X-ray Radioscopy to Investigate Metal Foaming, *Metals* 2 (2012) 10–21.
- [16] M. Mukherjee, Evolution of Metal Foams during Solidification, Ph.D. Thesis, TU Berlin, 2009.

- [17] A. Elmoutaouakkil, L. Salvo, E. Maire, G. Peix, 2D and 3D Characterization of metal foams using X-ray tomography, *Adv. Eng. Mater.* 4 (2002) 803–807.
- [18] Y. Yamada, T. Banno, Z. Xie, C. Wen, Characterisation of aluminium foams using x-ray computed tomography, in: N. Kanetake, H. Nakajima (Eds.), *Porous Metals and Metal Foaming Technology*, The Japan Institute of Metals, Sendai, 2006, pp. 419–422.
- [19] O.B. Olurin, M. Arnold, C. Körner, R.F. Singer, The investigation of morphometric parameters of aluminium foams using micro-computed tomography, *Mat. Sci. Eng. A* 328 (2002) 334–343.
- [20] M. Mukherjee, U. Ramamurty, F. Garcia-Moreno, J. Banhart, The effect of cooling rate on structure and properties of closed-cell aluminium foams, *Acta Mater.* 58 (2010) 5031–5042.
- [21] A. Meagher, M. Mukherjee, D. Weaire, S. Hutzler, J. Banhart, F. Garcia-Moreno, Analysis of the internal structure of monodispersive liquid foams by X-ray tomography, *Soft Matter* 7 (2011) 9881-9885.
- [22] Ghent University, Octopus – CT reconstruction software, <http://www.xraylab.com/>
- [23] M. Kobashi, R. Sato, N. Kanetake, Foaming and filling-in behavior of porous aluminum in hollow components, *Mater. Trans.* 47 (2006) 2178–2182.
- [24] F. Garcia-Moreno, N. Raffaele, J. Banhart, Optimisation of mould filling during PM metal foaming, in: G. Stephani (Ed.), "Cellular metals for structural and functional

applications (CELLMET2008), Fraunhofer-Institute IFAM, Dresden, Germany, 2008, pp. 133–138.

[25] G. Kaptay, On surface properties of molten aluminum alloys of oxidized surface, *Mater. Sci. For.* 77 (1991) 315–330.

[26] A. Dudka, F. Garcia-Moreno, N. Wanderka, J. Banhart, Structure and distribution of oxides in aluminium foam, *Acta Mater.* 56 (2008) 3990–4001.

Figure Captions

- Fig. 1.** Temperature course and projected foam area during expansion. Photograph shows the solidified foam. Vertical broken lines indicate transitions between different stages (I to IV) of foaming.
- Fig. 2.** Radioscopic images of a growing foam viewed in three different directions. Size of original precursor was $8.5 \times 8.5 \times 5 \text{ mm}^3$. (a) Foaming perpendicular to the mould base, (b) parallel to the mould base. (c) Same type of precursor as shown in (b) but tilted by 90° . The dashed black circle or ellipse indicate the geometric contour of the projected area of the expanded foam.
- Fig. 3.** Density profiles of foams that expanded in different directions in the mould. (a) perpendicular (corresponding to Fig. 2a, (b) parallel (Fig. 2b) to the mould base. The local relative density can be read both from the vertical axis and from the colour code.
- Fig. 4.** Radioscopic images of various stages of growth of originally wedge-shaped precursors (10 mm wide and high, 5 mm deep) oriented differently in the mould.
- Fig. 5.** Radioscopic images of expanding foams originating from two or three individual precursor pieces (each $8.5 \times 8.5 \times 5 \text{ mm}^3$ in size) oriented such that the foaming direction is the same for all the pieces. The photographs on the right side show the solidified foams.
- Fig. 6.** Series of radioscopic images of foams originating from different arrangements of precursor material pieces placed into the mould such that the

foam growth direction varied for the different pieces. (a) 3 rectangular samples (each $8.5 \times 8.5 \times 5 \text{ mm}^3$). (b,c) A combination of two rectangular ($8.5 \times 8.5 \times 5 \text{ mm}^3$) and one wedge-shaped sample (10 mm long, 10 mm diagonal, 5 mm thick).

Fig. 7. Rectangular foam sample ($16.55 \times 16.35 \times 11.6 \text{ mm}^3$ in size) obtained using multiple precursors with different foam growth directions. The black arrow indicates the joining region.

Fig. 8. 2D cross sections of 3D X-ray tomograms of some of the solidified foams ($16.55 \times 16.35 \times 11.6 \text{ mm}^3$ in size). Sections in (a, b, c) correspond to the plane shown in the radioscopic images for different arrangements in Fig. 6a, Fig 6b and Fig. 6c, respectively. Sections in (d, e, f) are perpendicular to (a, b, c). The small arrows indicate the joining regions.

Fig. 9. 3D tomographic reconstructions of the solidified foams ($16.55 \times 16.35 \times 11.6 \text{ mm}^3$ in size) shown in, (a) Fig. 6a, (b) Fig 6b, (c) Fig. 6c. The upper and lower sections in (a) and (c) correspond to the same plane or a plane perpendicular to that of the radioscopic images, respectively.

Table Captions

Table 1. Specification of the powders used to produce the precursor material.

Table 1. Specification of the powders used to produce the precursor material.

Powders	Supplier	Supplier specifications		Measured powder properties				
		Purity %	Range size μm	D10 μm	D50 μm	D90 μm	Mean diameter μm	Oxygen content %
Titanium hydride	Chemetall	99.00	<63	41.12	15.28	2.865	22	
AA 6061	Mepura	99.50	60-400	250	116	59	140	1.1
Nominal composition (wt.%) of AA 6061								
Al	Mg	Si	Cu	Cr	Mn	Zn	Fe	
Bal.	0.8–1.2	0.4–0.8	0.15–0.4	0.04–0.35	0–0.15	0.25	0.7	

Figure 1
[Click here to download high resolution image](#)

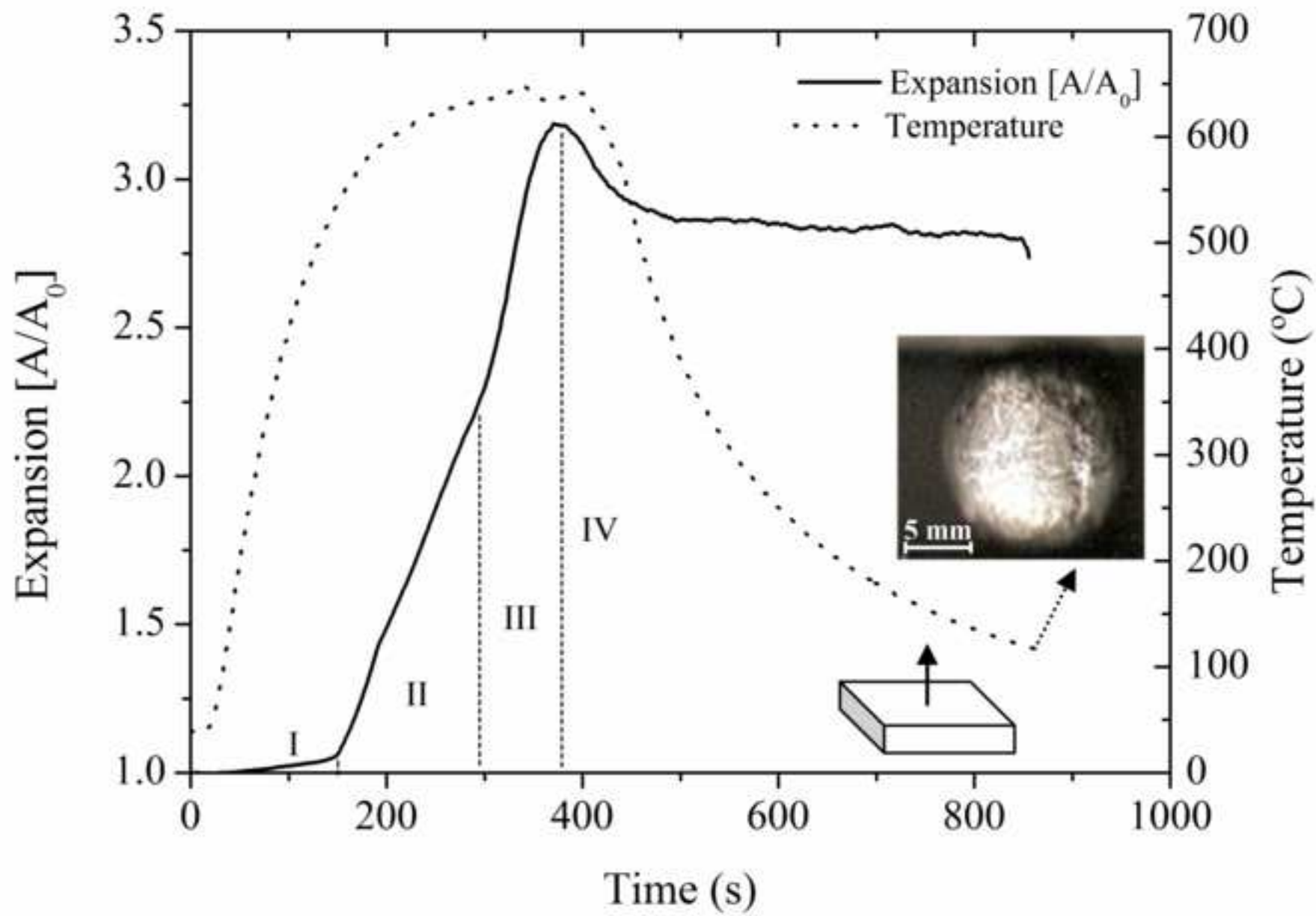
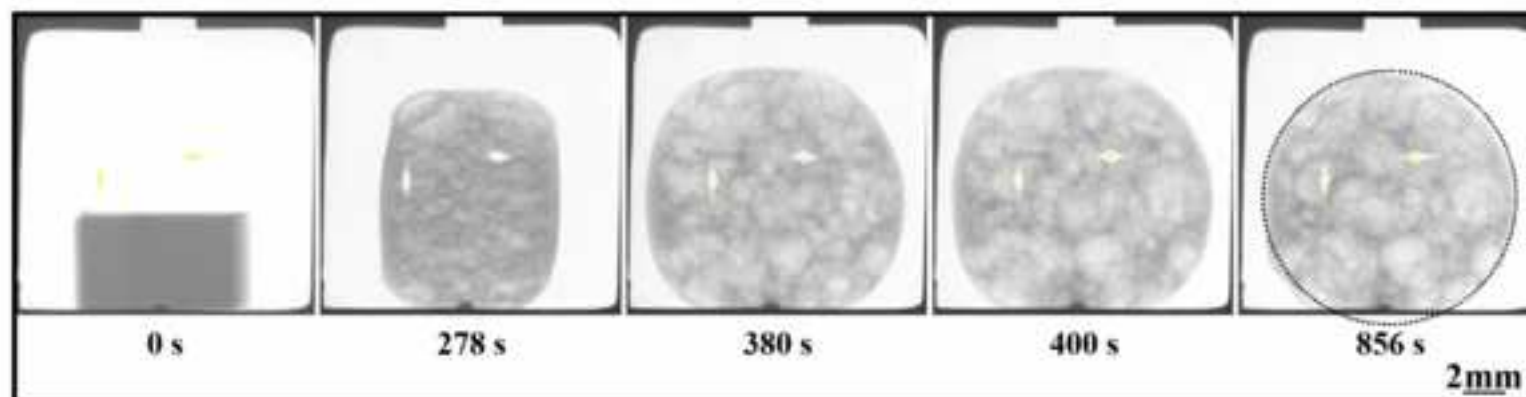
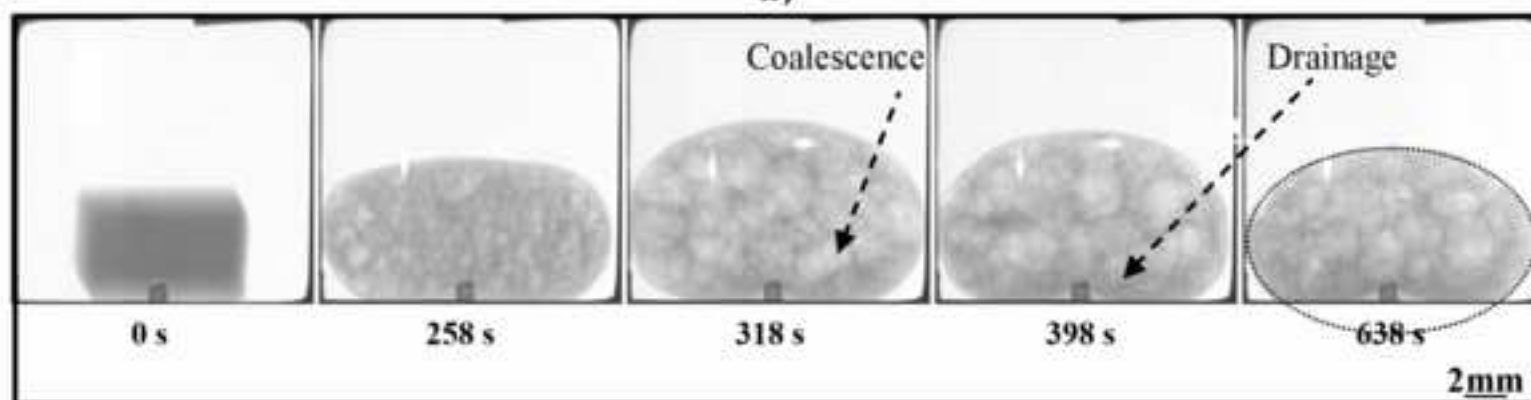


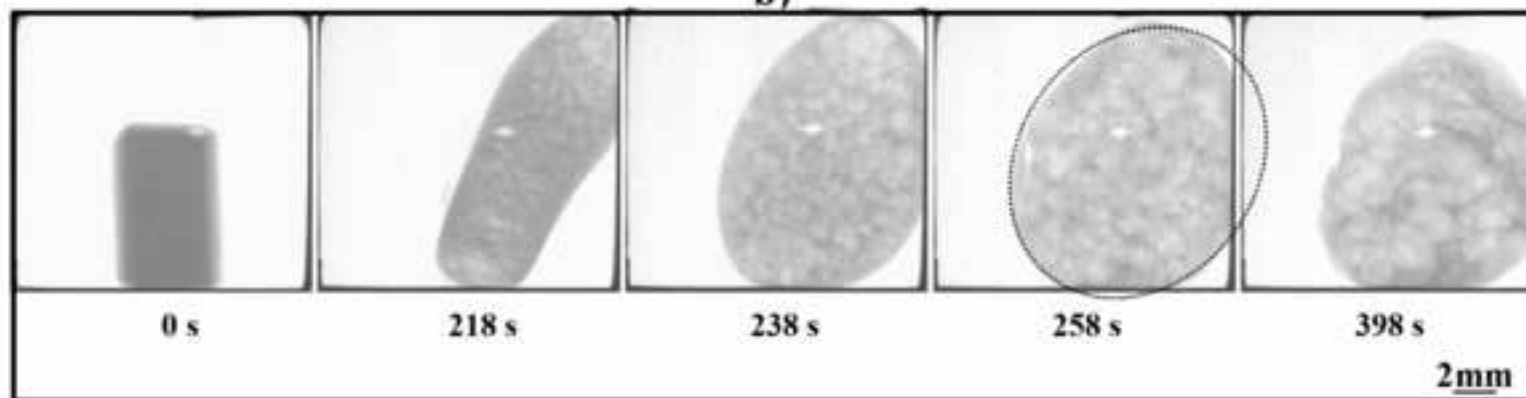
Figure 2
[Click here to download high resolution image](#)



a)



b)



c)

Figure 3
[Click here to download high resolution image](#)

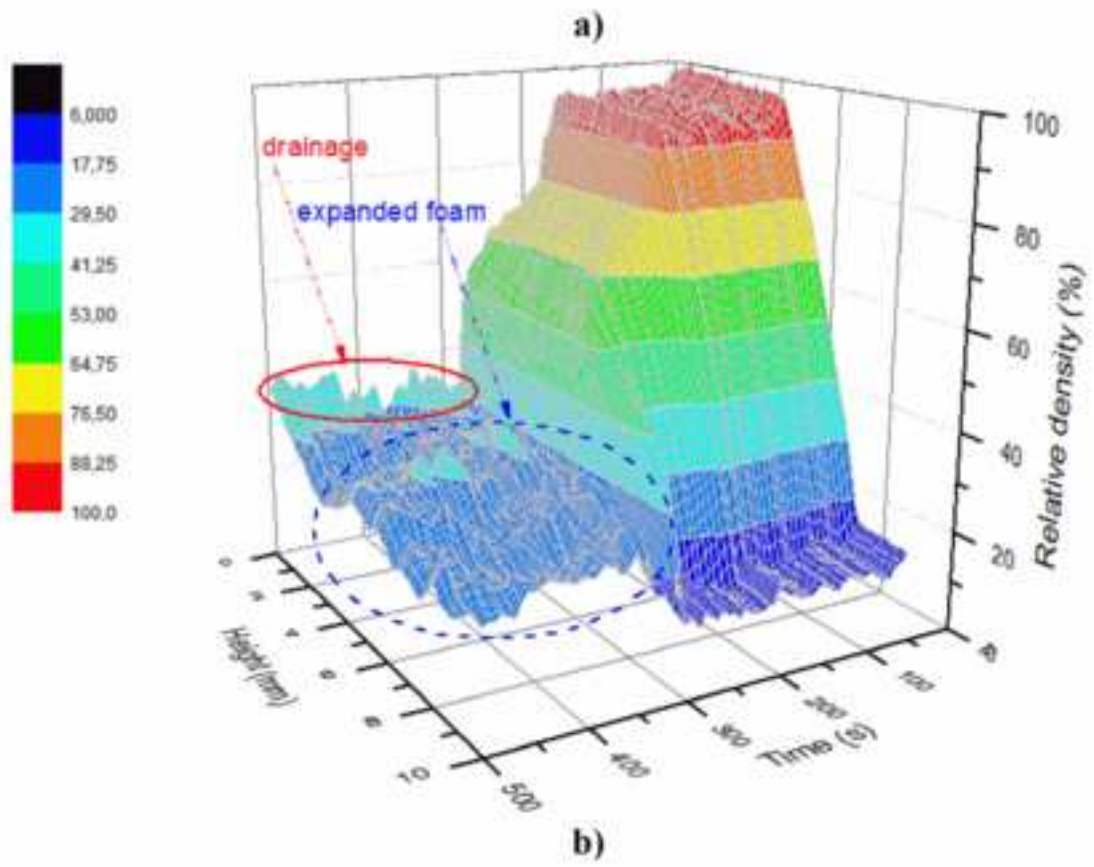
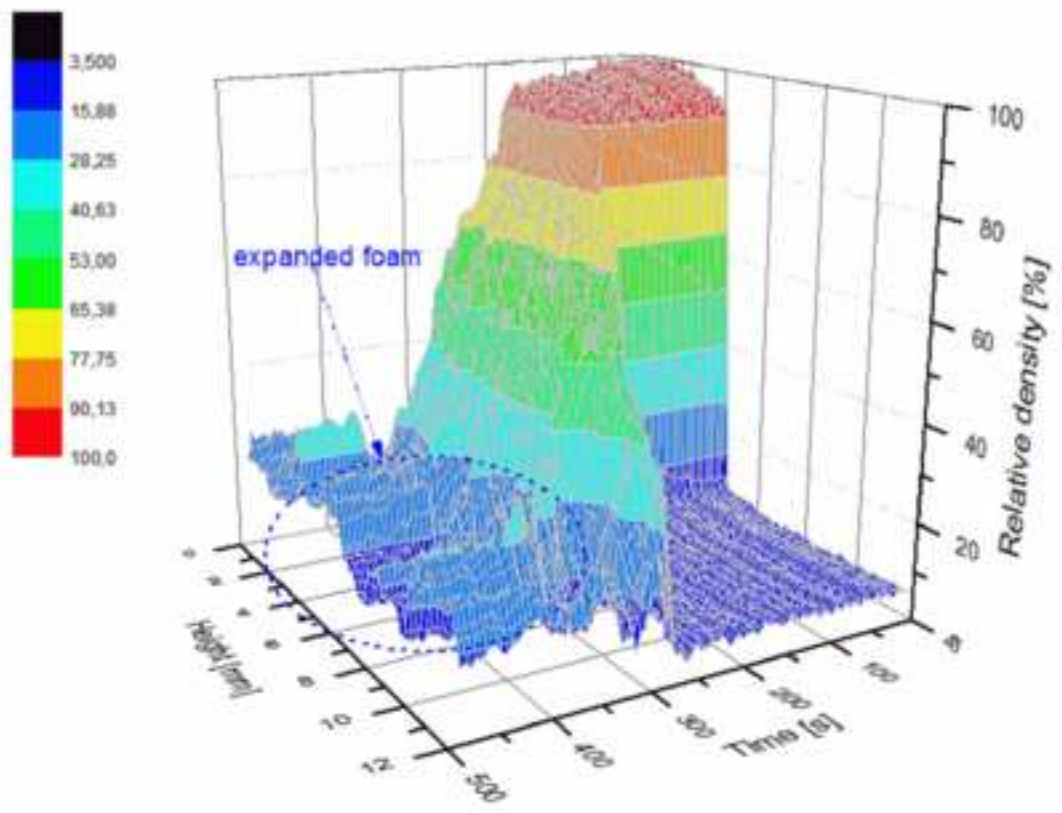
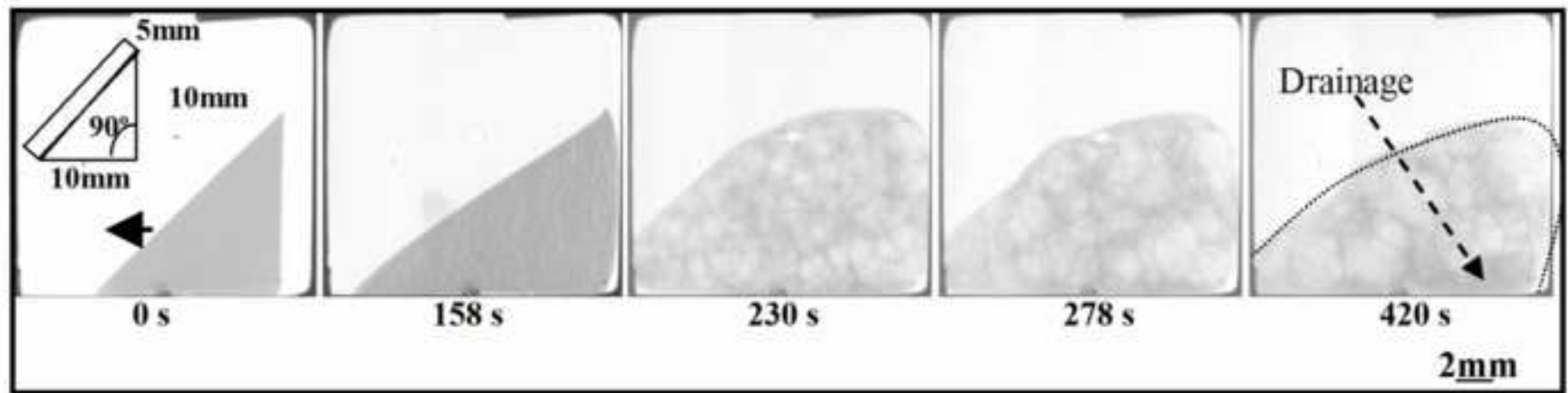
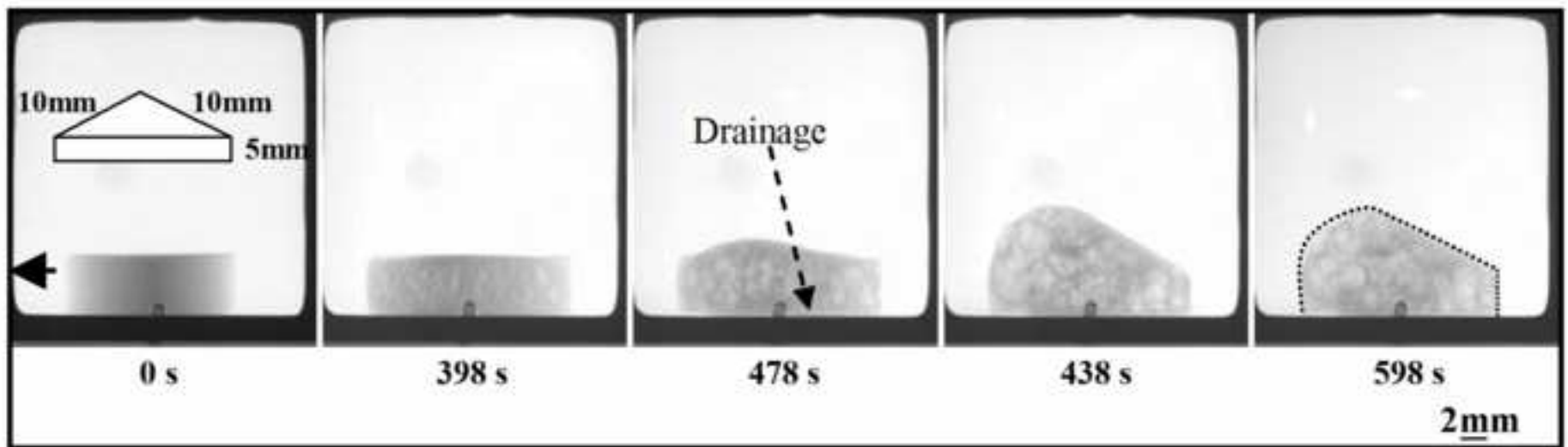


Figure 4
[Click here to download high resolution image](#)



a)



b)

Figure 5
[Click here to download high resolution image](#)

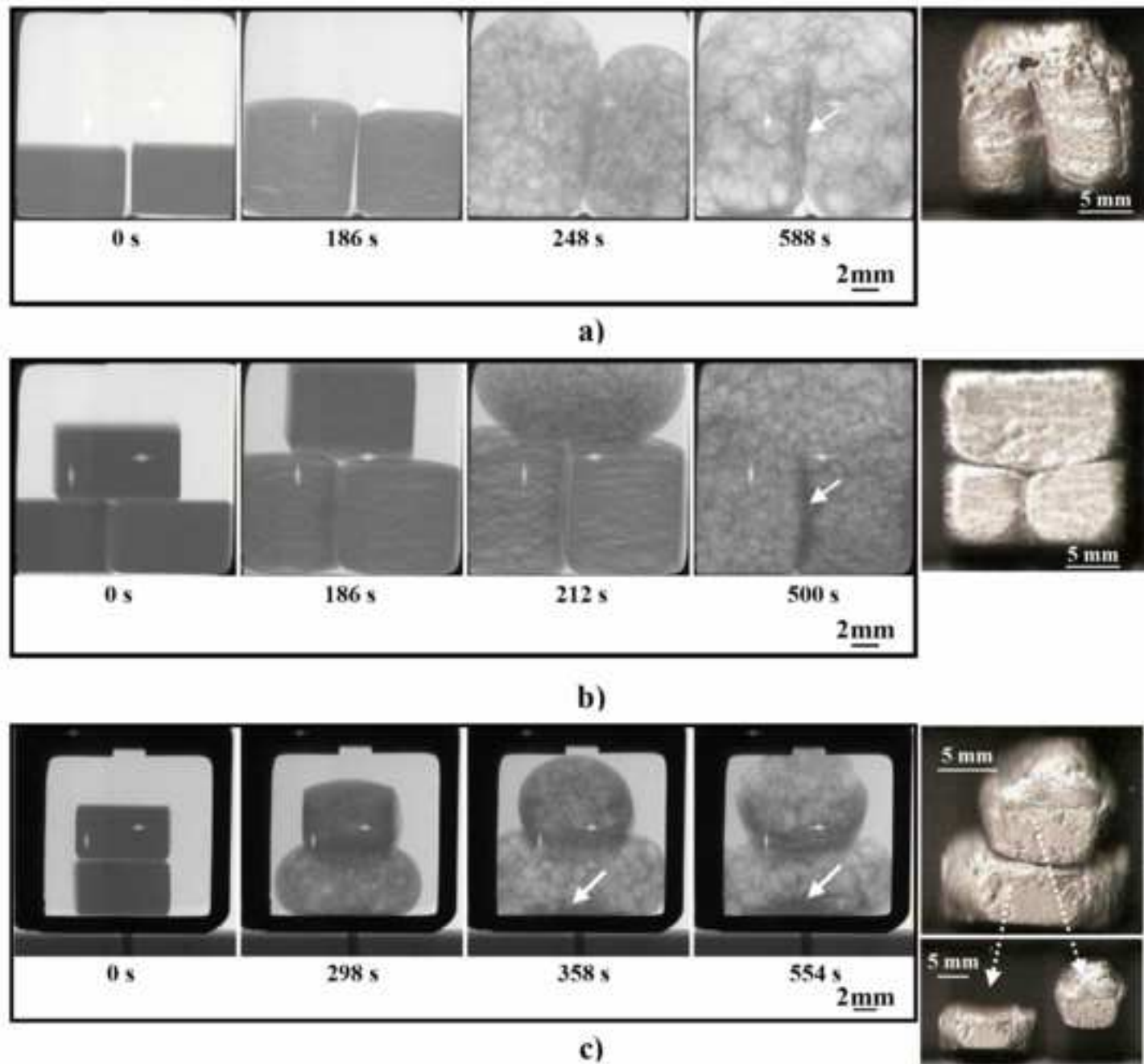


Figure 6

[Click here to download high resolution image](#)

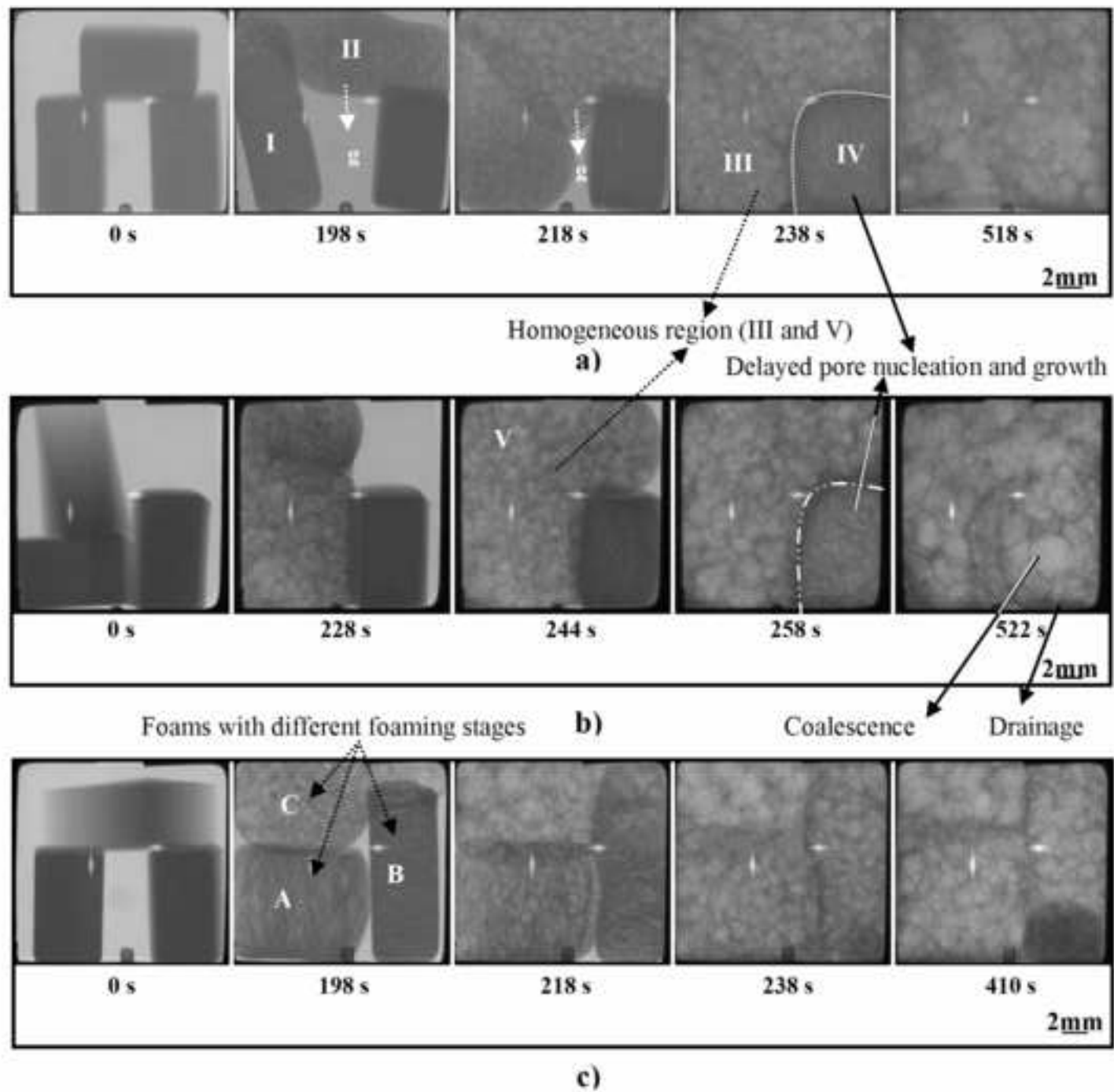


Figure 7
[Click here to download high resolution image](#)

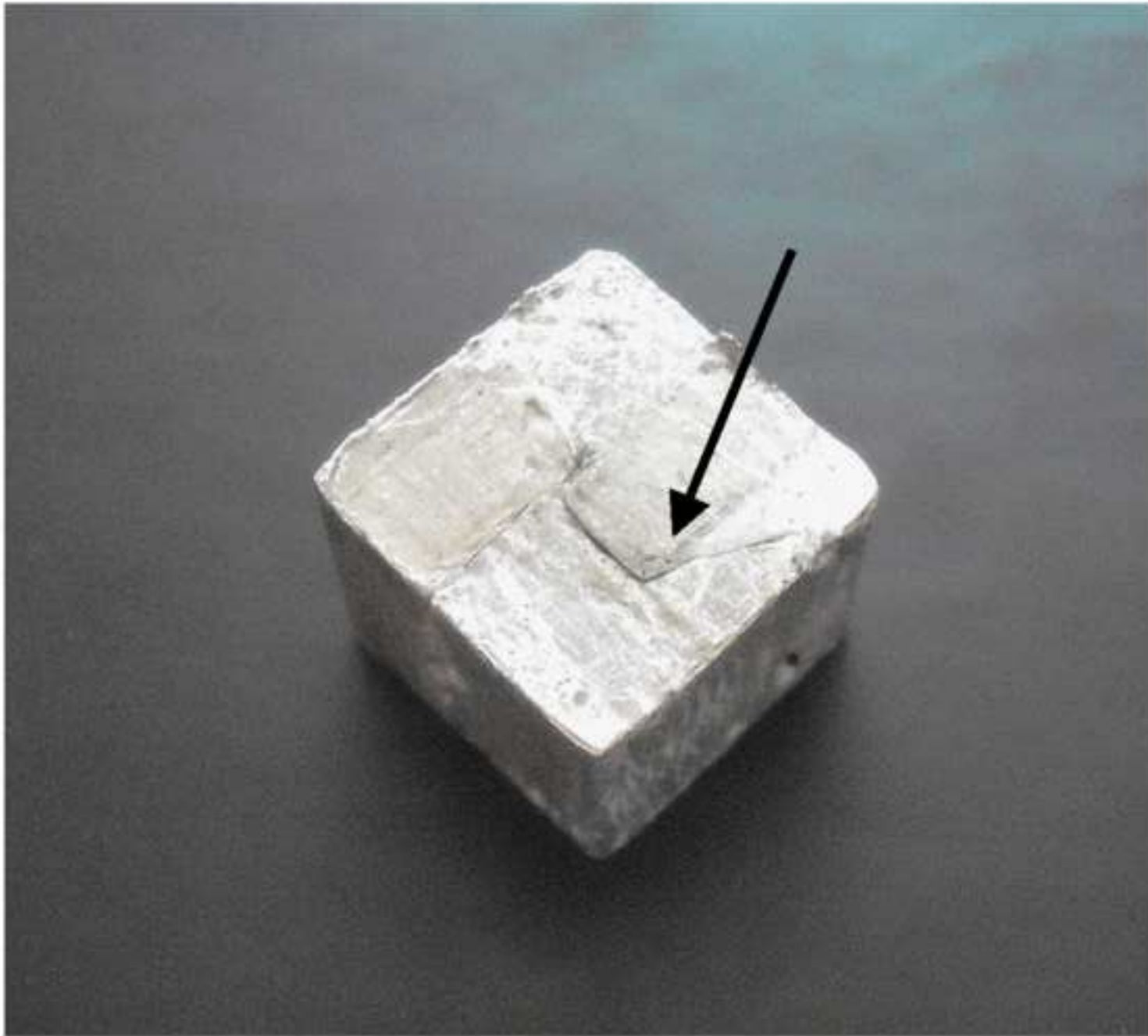


Figure 8
[Click here to download high resolution image](#)

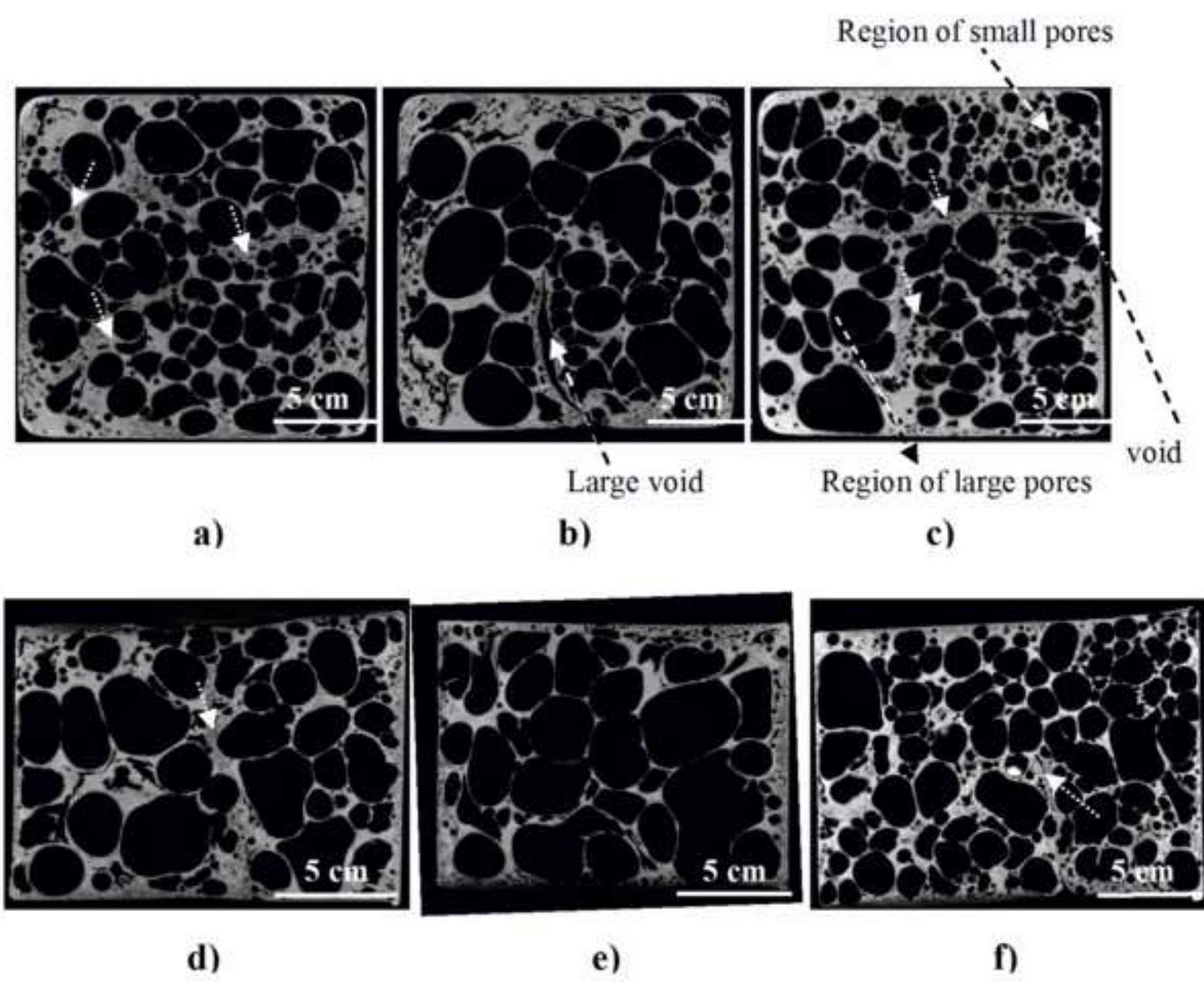
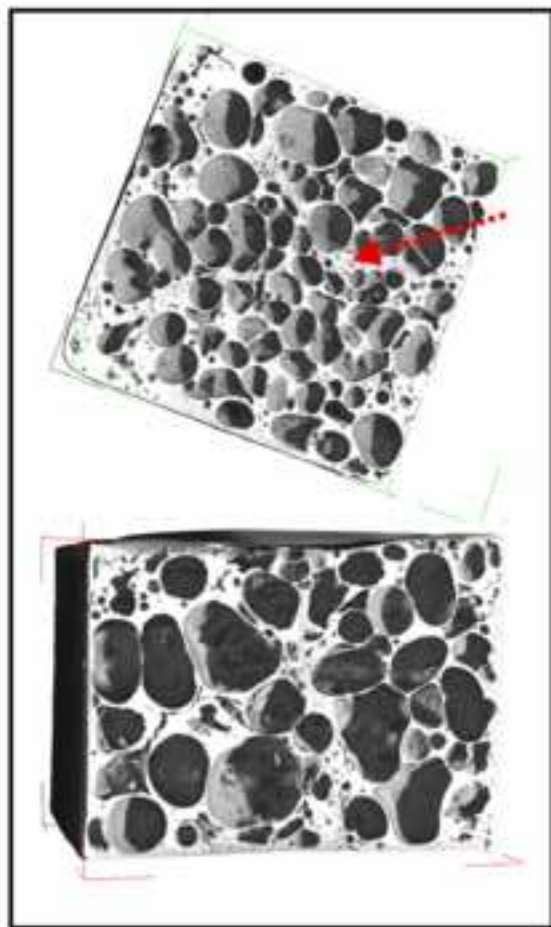
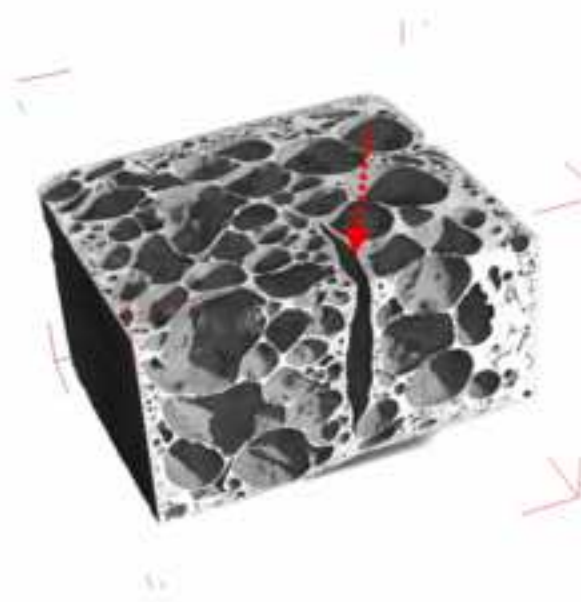


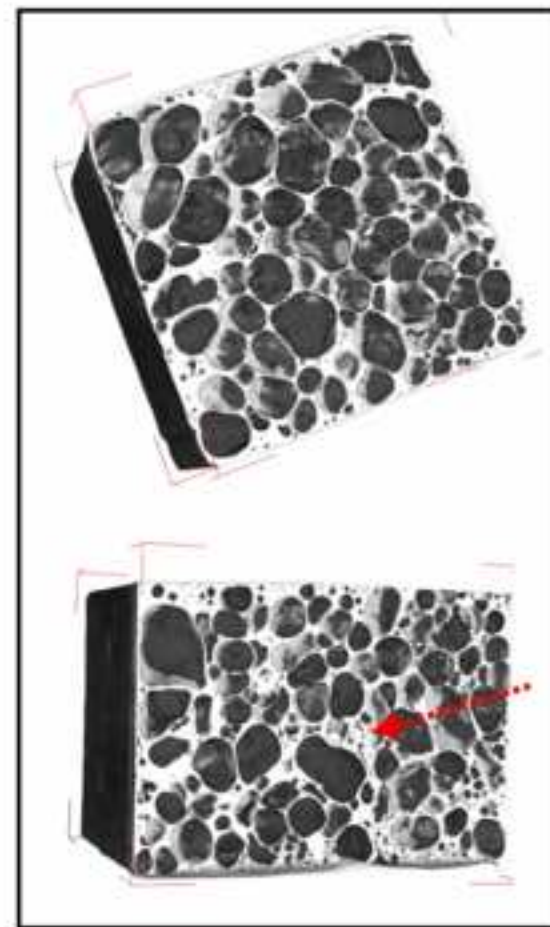
Figure 9
[Click here to download high resolution image](#)



a)



b)



c)